ELSEVIER

Wear 230 (1999) 39–55

WEAR

Failure modes of plasma sprayed WC–15%Co coated rolling elements

R. Ahmed [a,*], M. Hadfield [b]

[a] Cambridge University, Department of Engineering, Trumpington Street, Cambridge, CB2 1PZ, UK
[b] Bournemouth University, School of Design, Engineering and Computing, Tribology Design Research Unit, Studland House, 12 Christchurch Road, Bournemouth, BH1 3NA, UK

Received 22 July 1998; received in revised form 20 November 1998; accepted 23 December 1998

Abstract

This experimental study addresses the failure modes of plasma sprayed coatings in rolling contact. A high velocity plasma spraying system was used to deposit WC–15%Co coatings on the surface of 15 mm diameter 440-C bearing steel cones. These coatings were deposited in two different thickness. Rolling contact fatigue (RCF) tests were conducted using a modified four ball machine in conventional steel ball bearing and hybrid ceramic bearing configurations. These tests were conducted under various tribological conditions of contact stress and lubrication regimes at room temperature. Failure modes were investigated on the basis of surface and subsurface observations of failed coated rolling elements. Surface observations were made using conventional scanning electron microscopy (SEM) and light microscopy. Subsurface observations were made using fluorescent dye penetrant technique. Observations of debris generated during the RCF tests, changes in topography of lower planetary balls, electron probe microscope analysis (EPMA), microhardness/fracture toughness investigations and, coating microstructural studies are also included to aid the discussion. Two modes of failures, i.e., *surface wear* and *coating delamination*, were observed during this investigation. Coated rolling elements failed in either one or a combination of these two modes depending upon the tribological conditions during the RCF test. Surface wear was associated with asperity contact in the presence of microslip/sliding within the contact region. The process was accelerated in the later stages of RCF tests in the presence of wear debris due to additional mechanism of three body abrasion. Coating delamination was associated with the initiation/propagation of subsurface cracks, which resulted due to defects in the coating microstructure. These cracks propagated at the depths of orthogonal shear stress and maximum shear stress under the surface of wear track.

Keywords: Rolling contact fatigue; Tungsten carbide; Plasma spraying; Tribology; Failure modes

1. Introduction

The practical advantages of high deposition rates, low cost and, the versatility of coating a variety of materials on various substrate have enabled thermal spray coatings to become an integral part of aerospace, marine and, automobile industry. Among this family of coatings WC–Co coatings are known to provide the highest wear resistance in sliding contacts. The fatigue behaviour of these coatings in pure rolling or rolling/sliding contacts is however not thoroughly understood. This is because of the typical nature of thermal spraying process which results not only in anisotropic coatings containing varying levels of macro and micro residual stresses but also a variety of microstructural defects [1]. This lack of tribological understanding has so far limited these coatings to low stress applications.

Previous studies [2–8] on the fatigue behaviour of thermal spray coatings in rolling or rolling/sliding contacts have indicated that the performance is dependent upon the coating and substrate properties and the tribological conditions during the tests. However, not many investigations have been made on the tribological mechanisms leading to the failures of these coatings. Investigations of the failure mechanisms of these coatings can thus provide a better understanding of the tribological behaviour of these coatings in rolling sliding contacts. This study represents one such case in which the failure modes of plasma sprayed WC–15%Co coatings were investigated on the basis of the surface and subsurface investigations of the failed coated rolling elements. Surface observations were made using scanning electron microscope (SEM) whereas, subsurface observations were made using fluorescent dye

* Corresponding author. E-mail: ra222@eng.cam.ac.uk

0043-1648/99/$ - see front matter
PII: S0043-1648(99)00083-6

penetrations viewed under ultraviolet light. Results are discussed on the basis of debris analysis, coating microstructure, electron probe microscopy analysis (EPMA) and microhardness measurements of the coated rolling elements.

2. Test conditions and experimental test results

A modified four ball machine shown as Fig. 1 was used to investigate the rolling contact fatigue (RCF) performance of plasma sprayed (WC–15%Co) rolling elements. A Gator Guard plasma spraying system was used to produce the coated rolling element cones. The coated cone replaced the upper drive ball of the modified four ball machine and, represented the inner race of rolling element ball bearing. Coatings were produced in two different thickness on the surface of bearing steel (440-C) substrate having a diameter of 15 mm and apex angles of 109.4° and 90°. These coated rolling elements were ground and polished to attain a surface roughness of 0.1 ± 0.05 μm (R_q). Surface roughness measurements were made using a contacting type profilometer at 0.8 mm cut-off length. Details of the technique used to polish coated rolling elements can be seen elsewhere [2].

RCF tests were conducted under immersed lubrication conditions in conventional steel ball bearing and hybrid ceramic bearing configurations at a spindle speed of 4000 ± 10 rpm at an ambient temperature of 24°C. Failure was defined as the increase in vibration amplitude above a pre-set level. Two test lubricants Hitec-174 and Exxon-2389 were used in the testing programme. The ratio of the lubricant film thickness to average roughness (λ) was calculated using the following relationship:

$$\lambda = \left\{ H_{\min} / \left(R_{qd}^2 + R_{qp}^2 \right)^{0.5} \right\} \tag{1}$$

Where: R_{qd} was the surface roughness of the drive rolling element; R_{qp} was the surface roughness of the planetary ball; $H_{\min}$ was the minimum film thickness.

Minimum film thickness was calculated using the following relationship of hard elasto-hydrodynamic lubrication (EHL) [9], reproduced here for clarity:

$$H_{\min} = 3.63 U^{0.68} G^{0.49} W^{-0.073} (1 - e^{-0.68k}) \tag{2}$$

where: U = dimensionless speed parameter; G = dimensionless material parameter; W = dimensionless load parameter; k = dimensionless elipticity parameter.

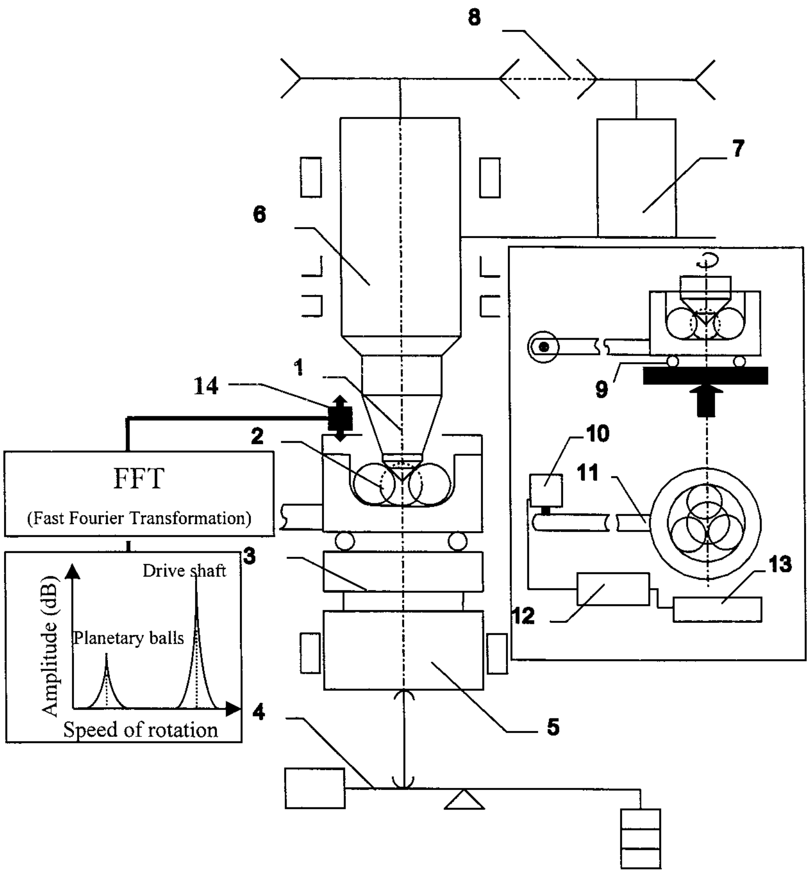

Fig. 1. Schematic of modified four ball machine. (1, Coated cone and collet; 2, planetary balls; 3, heater; 4, loading lever; 5, loading piston; 6, spindle; 7, driving motor; 8, belt drive; 9, thrust bearing; 10, force transducer; 11, torque arm for friction measurements; 12, digital readout; 13, printer; 14, accelerometer).

Table 1
Rolling contact fatigue test results for plasma sprayed coatings on 440-C steel substrate

Test no.	Average coating thickness (μm)	Lower balls	Contact stress[a] (GPa)	Contact width (b) (mm)	Depth of maximum shear (0.65 b) (μm)	Depth of orthogonal shear (0.4 b) (μm)	Lubricant	Sliding (%)	Frictional torque (N m)	No. of stress cycles (10^6)	Time to failure (min)	Type of failure
GG1AX	215	steel	2.74	0.132	85	52	Hitec-174	+2.3	0.0312	38.61	4290	surface wear
GG2AX	215	ceramic	3.1	0.124	80	50	Hitec-174	+2.8	0.015	9.891	1099	surface wear
GG3AX	260	steel	2.74	0.132	85	52	Exxon	+2.8	0.038	4.329	481	delamination
GG4AX	225	ceramic	3.1	0.124	80	50	Exxon	+2.8	0.003	0.891	99	delamination
GG5AX	260	steel	2.74	0.132	85	52	Dry	+0.3–9.6	0.06–0.17	0.891	99	surface wear
GG6AX	225	ceramic	3.1	0.124	80	50	Dye penetrant	+3.2	0.04	1.125	125	surface wear
GG1AY	60	steel	2.74	0.132	85	52	Exxon	+2.8	0.01	1.62	180	surface wear
GG2AY	70	ceramic	3.1	0.124	80	50	Exxon	+0.3	0.03	0.441	49	delamination
GG3AY	60	ceramic	3.1	0.124	80	52	Hitec-174	+2.3	0.097	0.180	20	delamination
GG4AY	50	steel	2.74	0.132	85	50	Hitec-174	+0.3	0.05	4.662	518	surface wear
GG1BX	140	ceramic	3.1	0.124	80	52	Hitec-174	−0.3	0.019	0.861	89	surface wear
GG2BX	140	steel	2.74	0.132	85	50	Hitec-174	−3.25	0.04	4.354	450	surface wear
GG3BX	140	ceramic	3.1	0.124	80	52	Exxon	−3.25	0.026	0.599	62	surface wear
GG4BX	130	steel	2.74	0.132	85	50	Exxon	−0.3	0.01	1.190	123	surface wear
GG1BY	90	ceramic	3.1	0.124	80	52	Exxon	−3.25	0.048	0.058	06	delamination
GG2BY	80	steel	2.74	0.132	85	50	Exxon	−3.25	0.036	0.870	90	delamination
GG3BY	90	ceramic	3.1	0.124	80	52	Hitec-174	−2.7	0.032	0.338	35	surface wear
GG4BY	90	steel	2.74	0.132	85	50	Hitec-174	−2.7	0.033	0.870	90	surface wear

[a]Uncoated case.

Using the above equations the λ value for the two lubricants was approximated as $\lambda > 3$ and $3 > \lambda > 1.5$ for the Hitec-174 and Exxon-2389 lubricants, respectively. In addition to these lubricants, tests were also conducted dry and using dye penetrant as test lubricant. The modified four ball machine was also instrumented to investigate the gross sliding in the four ball system and to measure the total frictional torque in the cup assembly. A description of the experimental test arrangements and the RCF test results have been made elsewhere [10]. The experimental test results are reproduced as Table 1 to aid the discussion. Contact stresses shown in Table 1 represent the uncoated case of contacting bodies. The orthogonal shear stress shown in Table 1 represents the stress acting on planes parallel and perpendicular to the surface and is the vector sum of q_{yz} and q_{zx}. Where, x-axis and y-axis are the major and minor axis of the contact ellipse, respectively, and, z-axis is normal to the contact ellipse. q_{yz} is the shear stress along z-axis on a plane normal to which is y-axis. q_{zx} is the shear stress along x-axis on a plane normal to which is z-axis. Details of the magnitude and location of these stresses can be seen from Engineering Science Data Units (ESDU, 84017) [11].

3. Surface observations

3.1. Failed coated rolling elements

Fig. 2 shows the surface observations of the failed rolling element used to conduct the test GG3AX. In this case the coating delaminated from within the coating microstructure at two locations. Fig. 2(a) shows the overall view of the wear track in SEI (secondary electron image) whereas Fig. 2(b) shows the same observation in BEI (back-scattered electron image). The BEI shows that the coating failure was from within the coating microstructure. Fig. 2(c) shows one of the delaminated areas of the coating at higher magnification. The rolling direction was from the left to the right of this figure and a crack can be seen at the leading edge of the delaminated coating. Fig. 2(d) shows the delaminated area at an inclined angle and the depth of the delamination can be appreciated as 45 μm.

Fig. 3 shows the surface observations of the rolling element subjected to the test conditions as described in the test number GG4AY. Fig. 3(a) shows the overall view of the failed area. The coating failure was due to the forma-

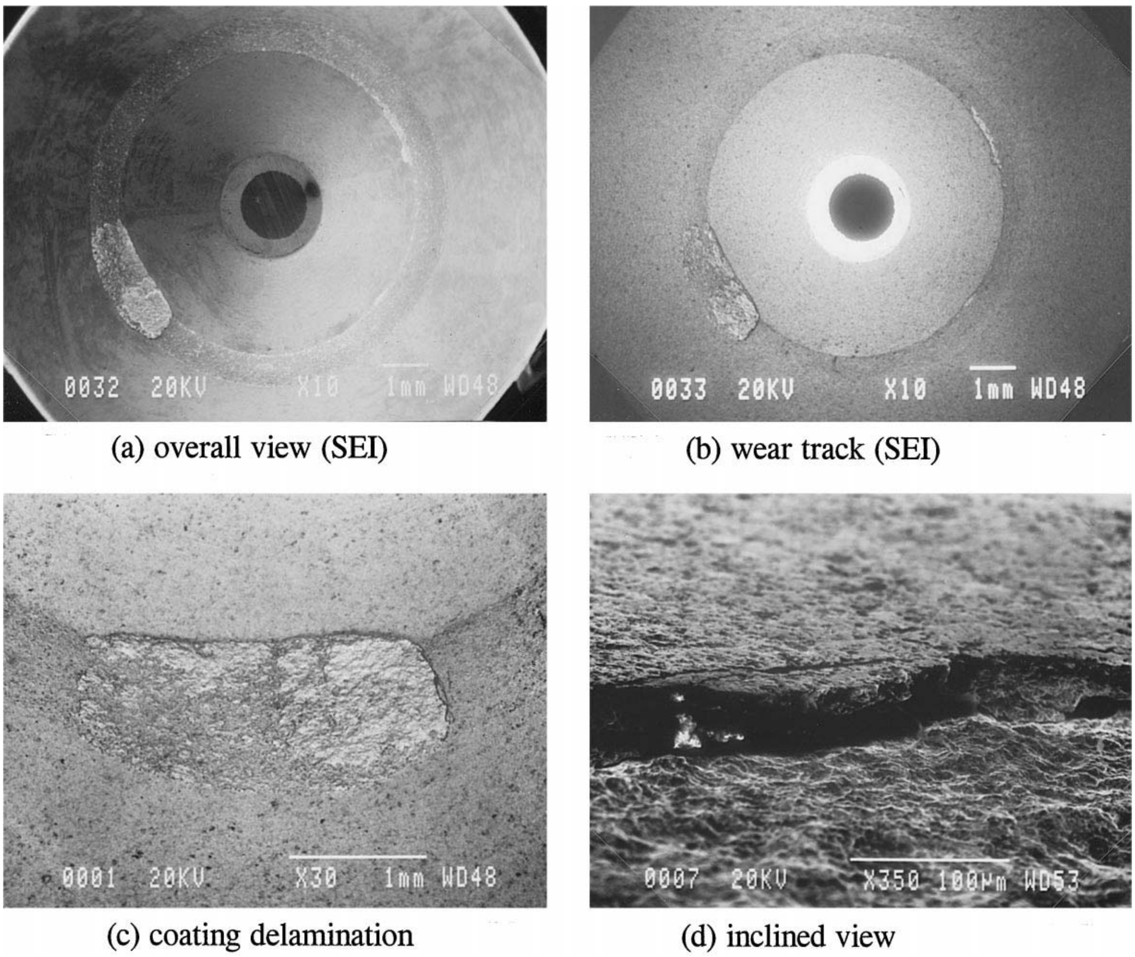

Fig. 2. Surface observations of the rolling element cone GG3AX.

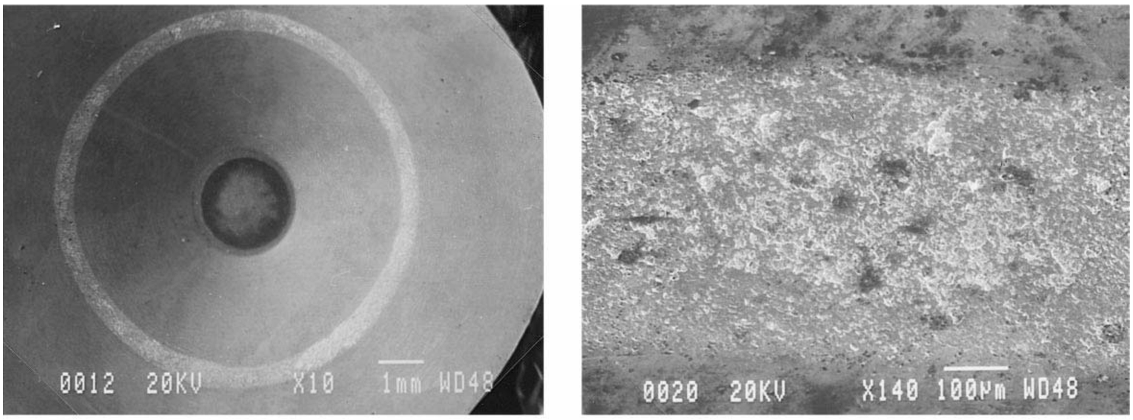

(a) overall view (SEI) (b) wear track (SEI)

Fig. 3. Surface observations of the rolling element cone GG4AY.

tion of micro-pits on the surface of the wear track as shown at a higher magnification in Fig. 3(b).

Fig. 4 shows the surface observations for the rolling element subjected to the test GG6AX. Fig. 4(a) shows the overall view of the wear track in SEI whereas, the BEI of the wear track is shown in Fig. 4(b). No delamination was observed in this case and the failure was similar to the surface observations of GG4AY (Fig. 3). This test was conducted to investigate the possibilities of lubricant entrapment mechanisms during the RCF tests.

Fig. 5 shows the surface observations of the rolling element cone subjected to the test GG2BY. Fig. 5(a) shows the overall view of the wear track in SEI, whereas Fig. 5(b) shows the same area in BEI. The atomic contrast image in BEI observation confirmed that the coating delaminated at the coating substrate interface at some locations and from within the coating microstructure at other locations. Fig. 5(c) shows the interfacial delaminated coating at higher magnification. Fig. 5(d) shows the inclined angle view of the delaminated coating. The depth of delamination can be approximated as 65 μm.

3.2. Debris generated during the RCF test

Fig. 6(a) shows the debris collected from the lubricant (Hitec-174) used for the test GG1AX [10]. EPMA analysis of the debris showed a mixture of W, Co and Fe which indicated that the debris were generated from the coated rolling element cone as well as from the lower planetary steel balls. Similar debris were seen for the tests which failed due to surface wear. Fig. 6(b) shows the surface observations of the debris collected from the lubricant (Exxon-2389) used for the test GG4AX [10]. These debris were in the form of thin sheet and few millimetres in length and width. The thickness of debris was approximated as 100 μm (Fig. 6b).

3.3. Planetary ball observations

Fig. 7(a) shows debris on the surface of the lower steel ball in BEI (test GG5AX). The size of the debris can be

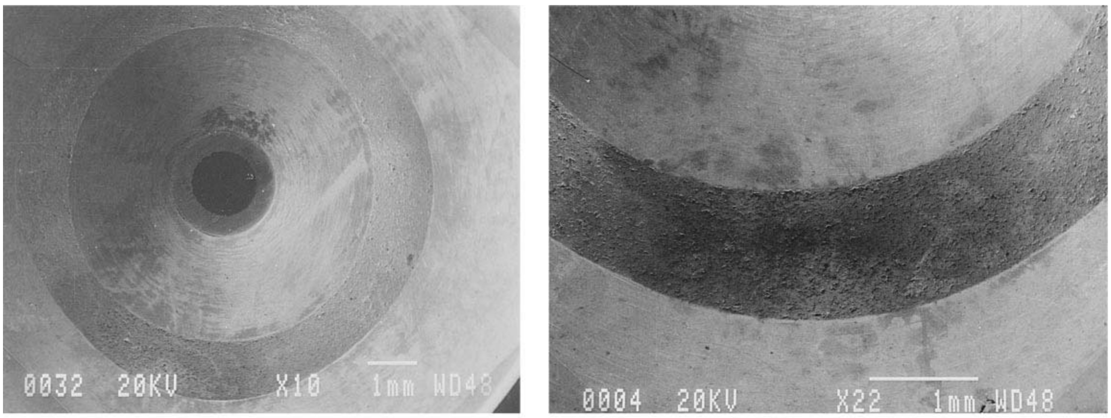

(a) overall view (SEI) (b) overall view (BEI)

Fig. 4. Surface observations of the rolling element cone GG6AX.

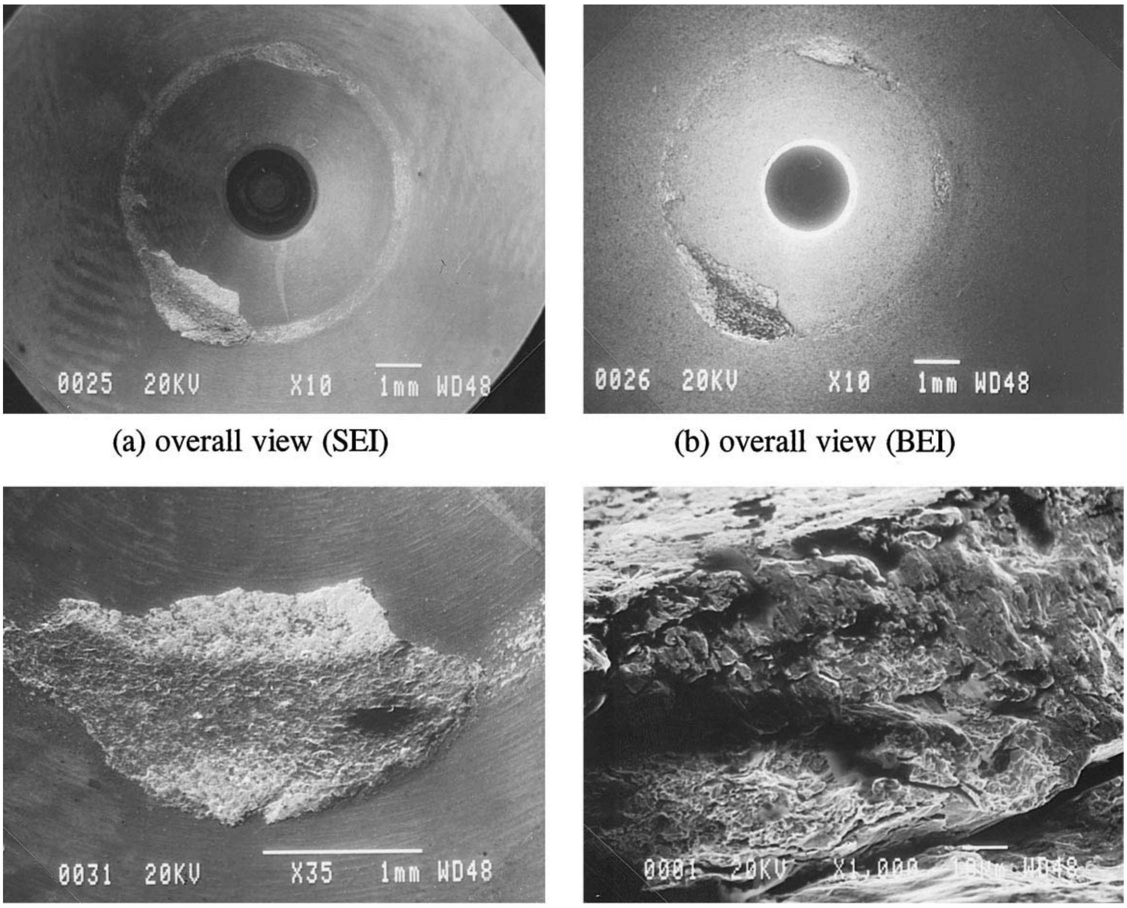

(a) overall view (SEI) (b) overall view (BEI)

(c) coating delamination (SEI) (d) inclined view (SEI)

Fig. 5. Surface observations of the rolling element cone GG2BY.

appreciated in the range of 5×3 μm to 1×1 μm. The EPMA analysis confirmed that these debris were W and Co. These debris were seen in abundance on the surface of the lower steel balls; however, the debris on the surface of the lower ceramic balls were very rare. Abrasion was also seen on the surface of the lower steel balls as shown in

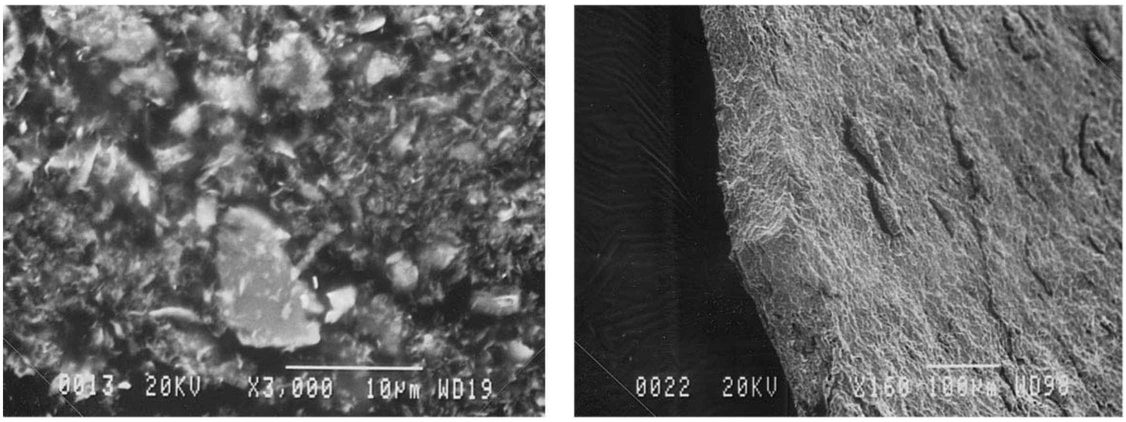

(a) overall view (SEI) (b) edge of delaminated debris

Fig. 6. Surface observations of the debris from the tests GG1AX and GG4AX.

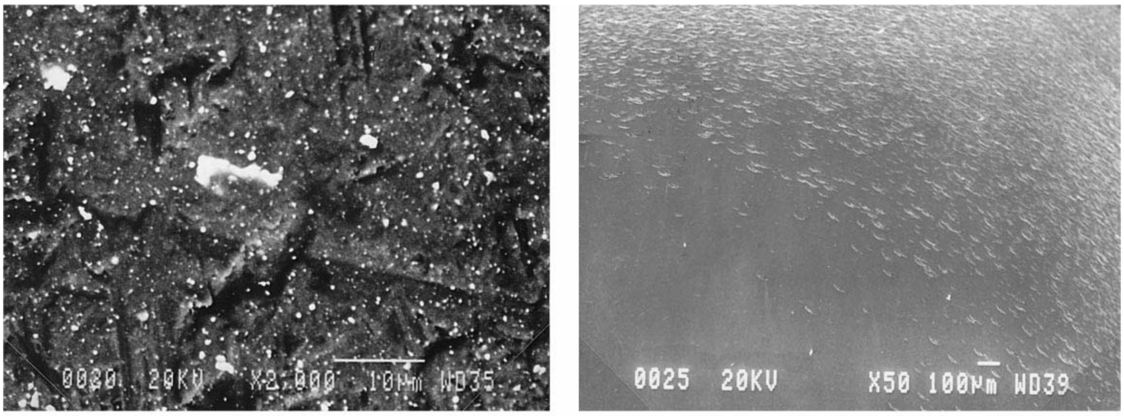

(a) debris on steel ball (BEI) (b) dents on the wear track (SEI)

Fig. 7. Surface observations of the planetary steel balls.

Fig. 7(b) (test GG1AX, [10]); however, this behaviour was not observed on the lower ceramic balls.

4. Coating microstructure

Fig. 8 shows the coating microstructure revealed after polishing the coating cross section using conventional polishing techniques. Fig. 8(a) shows the coating microstructure in SEI, whereas Fig. 8(b) shows the microstructure in BEI. It can be appreciated that the microstructure contains numerous pores and micro-cracks which can be seen within the WC particles. The existence of these microcracks and micropores was further verified by analysing the coating microstructure at higher magnifications. The atomic contrast images in the BEI indicated that there were secondary phase particles in the coating microstructure. The presence of secondary phase particles was confirmed by the EPMA analysis taken at points A, B, C and D (Fig. 8b). The darker angular particles as shown at point A indicated a strong peak of W and Co. At location B which was a much brighter phase resulted in a strong W peak only. This showed that at location A, some of WC reacted with Co during the plasma spraying process. This behaviour was consistent with the studies by Harvey et. al. (1995) [12]. They reported the formation of an amorphous W–Co–C phase due to the melting of WC–Co particles. At location B, however, it appeared that plain WC was present, which was indicative of either retained WC in the coating microstructure or the presence of W_2C particles. The EPMA analysis at location C indicated a strong Co peak indicating the Cobalt matrix. At location D, there were weak peaks of W, Co, etc., with a high background noise in the signal which was typical of porosity within the coating microstructure. The existence of various phases within the coating microstructure was further verified using X-ray diffraction analysis. The size

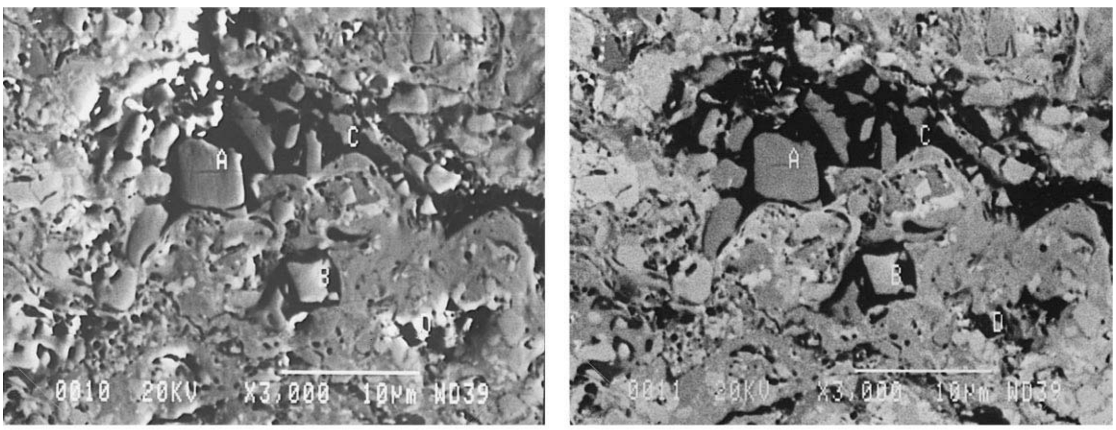

(a) coating microstructure (SEI) (b) coating microstructure (BEI)

Fig. 8. Coating microstructure.

of angular WC or W_2C particles was approximated to be in the range of 2×2 μm to 10×5 μm. These observations indicated that the coating microstructure contained a mixture of defects such as micro-pores, micro-cracks and secondary phase particles, etc. These defects were seen not only at the interaction of lamellas within the coating but also at the coating substrate interface. No attempt was made to quantify the level of porosity in the microstructure.

Although the investigation of coating microstructure in this study was limited to show the existence of micro-pores, micro-cracks and secondary phase particles, thermal spray coatings are also prone to a variety of other microstructural defects. Some of these defects can be seen from Wilms [13] and Kudinov et al. [14]. In general, coating microstructure is complex and not only depends upon the viscosity, temperature, velocity and wettability of impacting lamella but also on the thermal conductivity, tempera-

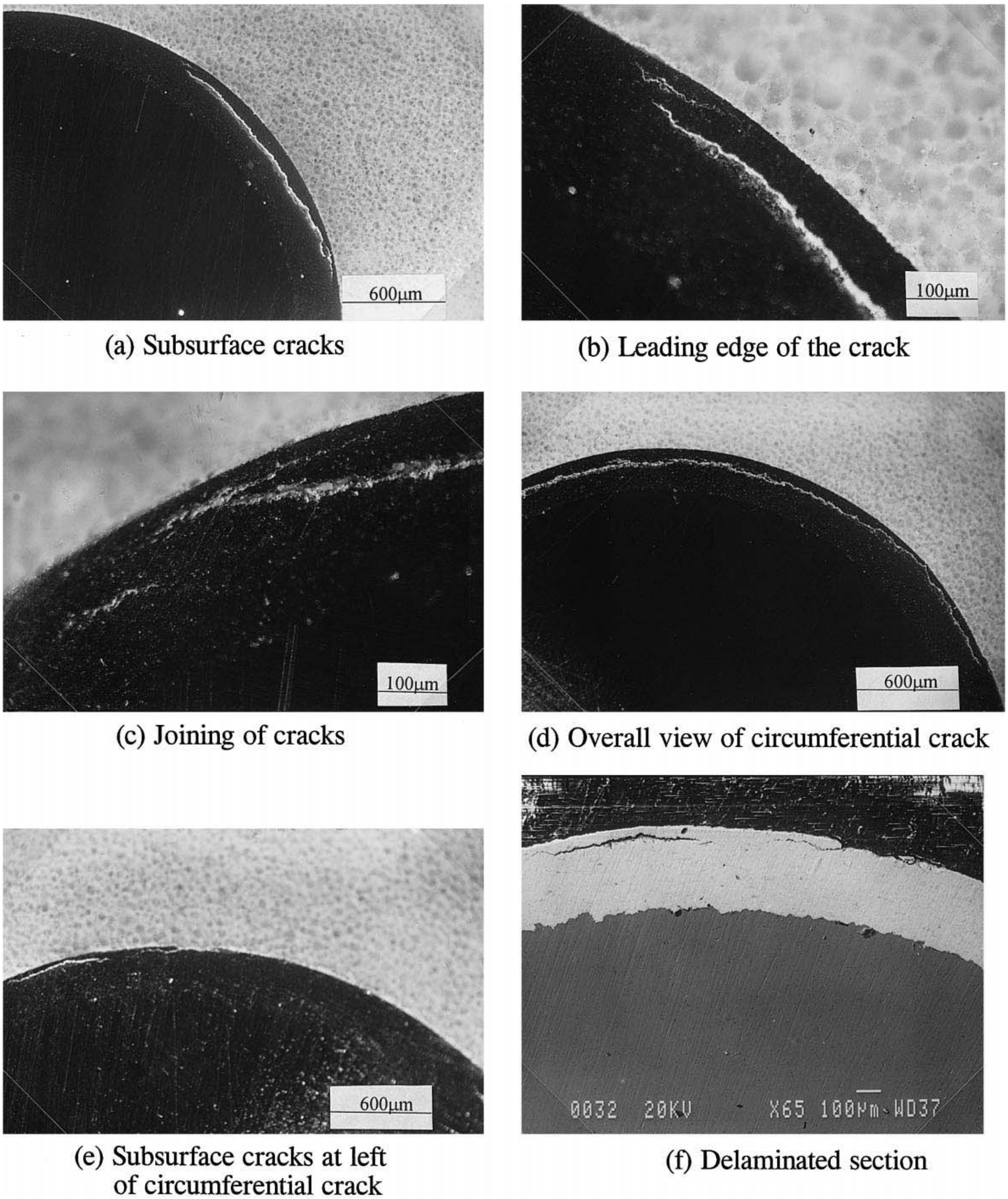

Fig. 9. Subsurface observations (GG3AX).

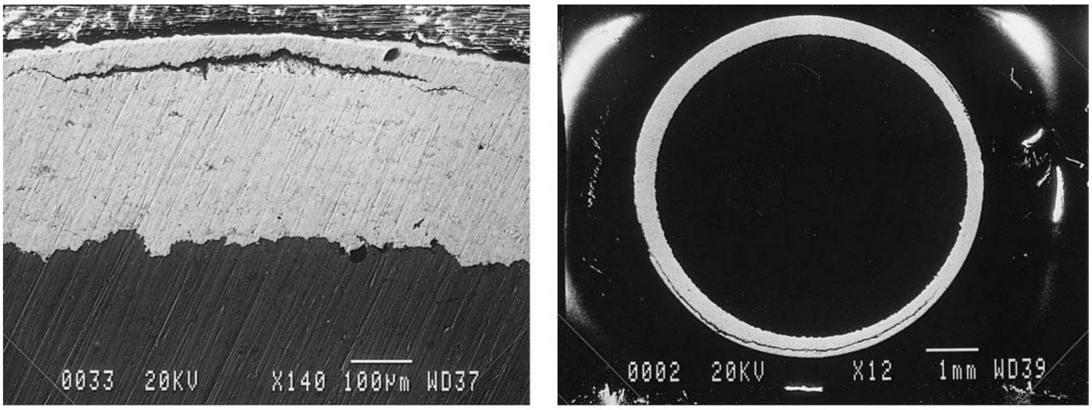

(g) Other cracks (h) Subsurface circumferential crack

Fig. 9 (continued).

ture and surface roughness of underlying substrate or lamella. The investigations of the influence of these factors on the coating microstructure were beyond the scope of this work.

5. Subsurface observations

The surface observations of the failed rolling elements described in Section 3 could be useful in understanding the types of tribological failures during the RCF tests. However, the understanding of mechanisms, which could possibly lead to different types of tribological failures could not be explained without exploring the subsurface changes during the RCF tests. This is because the mechanisms, such as slip (gross sliding and micro-slip), tribological behaviour of surface asperities during the various rolling contact configurations and, some of the key contact stresses like peak compressive and tensile stress appear on or near the surface of the contacting bodies. These factors can be thought responsible for the surface or near surface changes seen during the surface investigations. However, the shear stresses such as the maximum shear stress and, the orthogonal shear stress appear at certain depths under the surface of the rolling elements. These depths depend upon the contact stress and the tribological conditions during the test. Subsurface investigations were therefore essential to explore the role of those shear stresses during the RCF tests.

5.1. Methodology of subsurface investigations

Subsurface cracks under the wear track were investigated by sectioning (grinding) of the rolling elements along the axis of the rolling element cone. One of the problems, which had to be tackled for these investigations, was the generation of cracks during the sectioning process. The brittle and lamella microstructure of thermal spray coatings made it very difficult to section these rolling elements without generating cracks using conventional sectioning techniques such as diamond saw sectioning. To overcome this problem, an alternative route was selected by progressively grinding the rolling element at the location of the wear track using silicon carbide paper (grid 800 to 1200). Grinding was carried out successively along the axis of the cone. This was a slower, tedious but gentle process than the conventional diamond saw sectioning process. The coating was therefore less prone to cracking during the grinding process. This technique also had the advantage of removing very thin layers of material, which were difficult to remove with the diamond saw sectioning technique.

However, even with this gentle process there was no guarantee that the grinding of the rolling element cones would not alter the subsurface microstructural changes such as cracks produced during the RCF test. To confirm that the subsurface changes (cracks) were generated during the rolling contact and not due to the grinding of the rolling elements, the rolling elements were examined for subsurface cracks using the fluorescent dye penetrant technique. In this technique, failed rolling elements were cleaned in acetone and petroleum spirit in ultrasonic bath. These rolling elements were then immersed in a fluorescent dye prior to grinding. Excessive dye from the surface was removed using a dye remover. The fluorescent dye and dye remover were of commercial grade. Subsurface investigations were then made using ultraviolet light and white light during successive grinding.

5.2. Crack observations

Fig. 9 shows the subsurface observations of the rolling element cone used for the test GG3AX. The surface observations of this rolling element (Fig. 2) indicated that the rolling element delaminated from within the coating microstructure. Fig. 9(a) shows subsurface cracks observed under the ultraviolet light just before the edge of wear track. Three different cracks were visible at two different depths under the surface of the wear track. The big crack in the middle can be seen at a deeper depth while two hairline cracks can be seen appearing on either end of the big crack at a shallower depth. Considering the magnification of the image and taking account of the apex angle, the coating thickness was approximated as 260 μm. Similarly, the maximum depth of the big crack and the short shallow cracks on either ends for the contact was approximated as 90 μm and 45 μm, respectively. The rolling direction was from the right to the left of the figure. Fig. 9(b) shows the leading edge of the big crack at a higher magnification. Two independent cracks at two different depths can be seen clearly at this magnification.

Fig. 9(c) shows subsurface observations after some more grinding along the axis of the rolling element cone into the wear track. The cracks extended in length in both directions and joined together. Another short and independent subsurface crack also appeared on the left of the big crack at a contact depth of approximately 90 μm. As the progressive grinding through the wear track continued the big crack extended in length in both directions either independently or by joining other cracks as shown in Fig. 9(d). Apart from the propagation of this big crack, new independent cracks appeared under the surface of wear track as shown in Fig. 9(e). This crack emerged on the left of big crack which is visible on the right of figure. It was found that this crack lead to the delamination of rolling element from within the coating microstructure. These fluorescent dye investigations confirmed that these cracks were generated during the RCF and not due to the sectioning process, SEM observations were made on these cracks for analysis at higher magnifications. Fig. 9(f) shows the crack associated with the delaminated section of the coating. The depth of failure can be approximated as 45 μm. New cracks were also visible at this depth as shown at a higher magnification in Fig. 9(g). These cracks ultimately joined together with the big crack during the RCF test to form a long circumferential crack as shown in Fig. 9(h).

Fig. 10 shows the subsurface observations of the coated rolling element cone used for the test GG2BY. The rolling element failed because of the coating delamination at the interface (Fig. 5). Subsurface interfacial (coating/substrate interface) cracks were observed at the edge of the wear track. Fig. 10(a) shows a view of these cracks under ultraviolet light whereas, Fig. 10(b) shows these cracks at another location at a higher magnification. Using basic trigonometric relations the contact depth of these interfacial cracks was approximated as 70 μm. As more grinding was carried out along the axis of the cone, these subsurface cracks reached the surface exposing the delaminated area

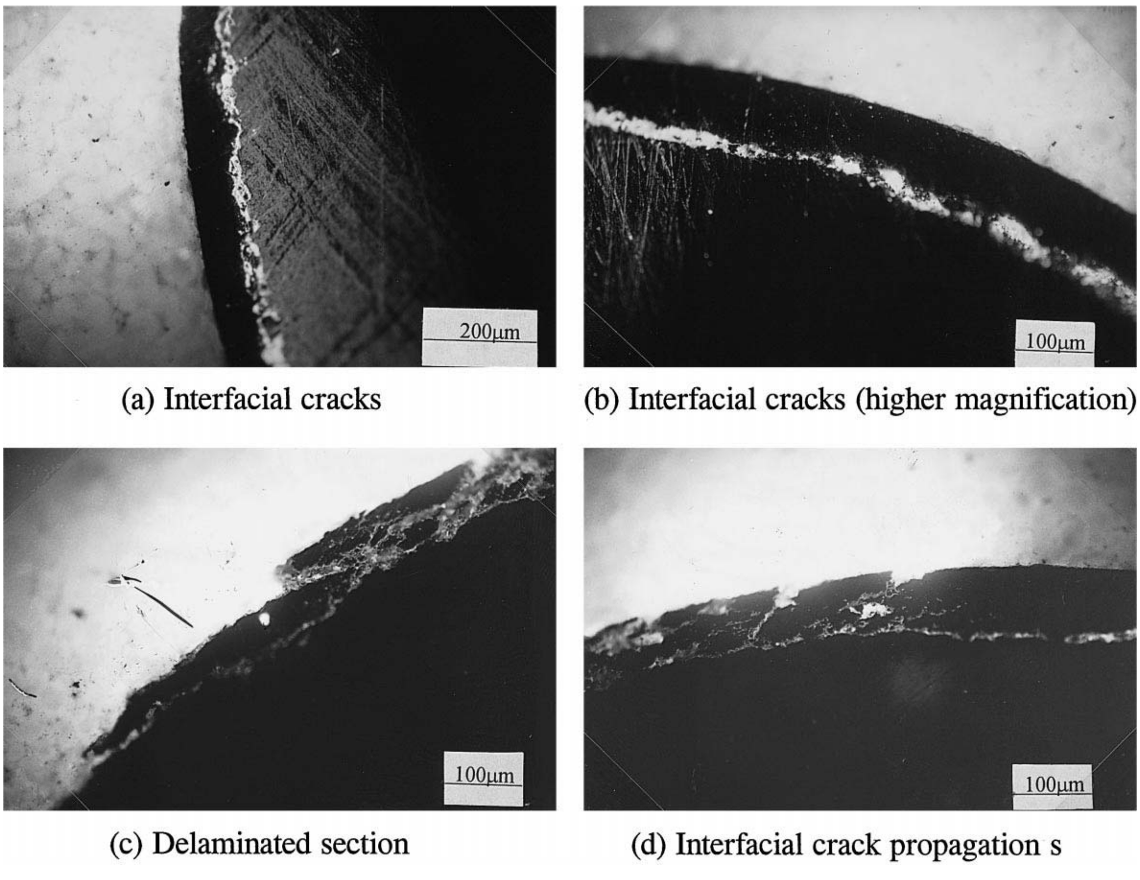

Fig. 10. Subsurface observations (GG2BY).

of the coating. Fig. 10(c) shows these subsurface cracks under the delaminated section of the coating. The coating delamination can be observed at two different depths under the surface of the wear track, i.e., (i) at the coating substrate interface as seen on the left of the figure and (ii) from within the coating microstructure at a contact depth which was approximated as 30 μm. The rolling direction was from the right to the left of the figure. It can be appreciated that if these cracks were thought to initiate and propagate from the surface towards the interface of the coating, they must have propagated in the direction opposite to rolling. However, if the cracks initiated and propagated from subsurface to surface then the direction of propagation was in the direction of rolling at the leading edge of the contact and visa versa at the trailing edge of the contact. Fig. 10(d) shows few other interfacial cracks which reached the surface.

6. Microhardness measurements

A Knoop and scratch hardness tester was used to measure the micro-hardness of plasma sprayed rolling element cones. The microhardness results indicated that the average micro-hardness of the coating material was 1158 (HV_{300}) and 1139 (HV_{200}). The average microhardness of the substrate material was measured as 700 (HV_{100}). These values were averaged for 12 readings after neglecting the highest and the lowest values.

Attempts were also made to study the indentation fracture toughness (K_{1c}) and the critical strain energy release rate (G_c) of thermal spray coatings using the diamond indentation technique. However, even after repeated attempts and extreme care in preparing the surface for microhardness indentations, it was not possible to obtain a reliable value of K_{1c} or G_c. It was mainly because the coating cracked at some locations at an indentation load of 100 p and at other locations at load of 300 p or 500 p. Fig. 11(a) shows a typical result in which the coating cracked at an indentation load of 300 p. Moreover, the cracks did not satisfy the criteria ($C > 2b$, where C is the crack length and b is the diagonal of indentation). The cracks did not always originate from the notch of the diamond indentation but also from the sides of indentation. This indicated that the stress concentrations at the pores and micro-cracks within the coating microstructure were higher than the theoretically applied load, which caused these cracks to originate and propagate during the indentation process. Some of these observations are shown in Fig. 11(b).

7. Discussion

The main objectives of this experimental study were to classify the types of tribological failures observed on the surface of failed coated rolling elements and, to identify the tribological mechanisms leading to these failures. Surface observations of plasma sprayed coatings indicated that the failures observed on the surface of coated rolling element cones can be classified into two main categories, i.e., *surface wear*, and *subsurface delamination.* The rolling elements failed in either one of these types of failures or a combination of two depending upon the tribological conditions prevailing during the RCF tests. These two types of failures and the related tribological mechanisms are discussed below.

7.1. Surface wear

Surface wear was the failure mechanism seen with both the lubricants in all the cases of the RCF tests (Table 1). In some cases, this type of failure was observed along with the delamination type of failure whereas, in other cases, this was the only mechanism of coating failure. In Table 1, only those failures are marked as surface wear in which

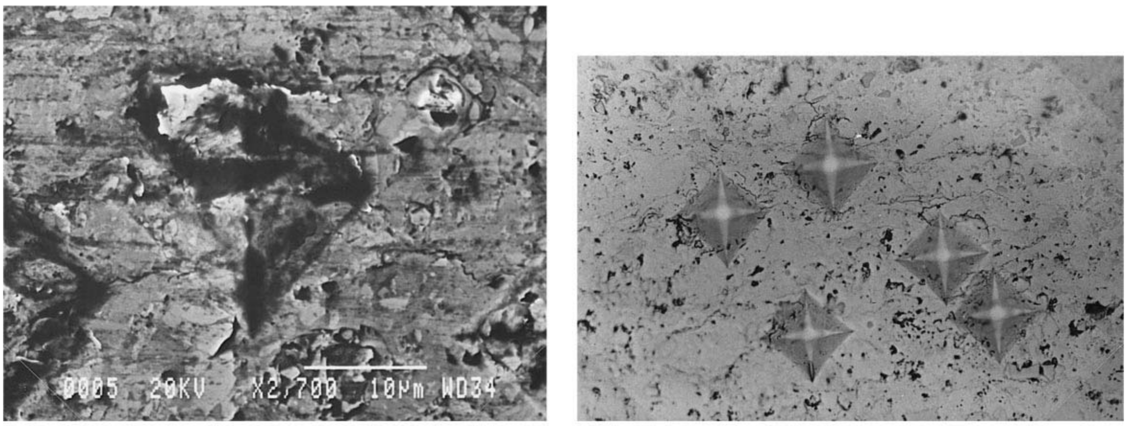

(a) Indentation at 300p (SEI) (b) Indentations at 500p

Fig. 11. Micro-hardness indentations.

this was the only failure mechanism. Figs. 3 and 4 represent some of the cases in which surface wear was mainly responsible for the failure of rolling elements. In this type of failure, numerous micropits appeared on the wear track of coated rolling element. These micropits were similar to the micropits seen on the worn gear and bearing surfaces and resulted from the interaction of surface asperities.

In this type of failure, a shallow wear track was formed the depth of which varied depending upon the contact configuration and the time to failure. As a result of this surface wear the contact became conforming and the width of wear track increased. This can be observed from Figs. 3 and 4 in which the width of the wear track during the RCF tests increased from an initial value of 132 μm (test GG4AY, Table 1) and 124 μm (test GG6AX, Table 1) to 400 μm and 1000 μm, respectively. This indicated that the contact stress also decreased due to contact conformity from 2.7 and 3.1 GPa to 1.0 and 0.5 GPa for the two cases. Similar trend was observed for the other cases. Small wear debris of the type shown in Fig. 6(a) were produced during this type of failure. Small pits of the type shown in Fig. 3(b)Fig. 4(b) were produced on the surface of the wear track. Cross-section examination of these pits revealed that the depths of these pits were in the range of 5 to 10 μm.

7.2. Mechanism of surface wear during RCF tests

This type of failure was mainly due to the asperity contact in the presence of gross sliding and microslip within the contact region and, due to the action of wear debris generated during the RCF tests. This mode of failure was thus surface initiated due to the micro-fracture or plastic deformation of asperities and resulted in the micro-pitting of surface. When the lubrication conditions were in the mixed region ($\lambda < 3$) surface asperities came into contact. The presence of gross sliding and microslip within the contact region provided a tangential force at the junction of asperities. This tangential force produced small debris due to conventional wear mechanisms like ploughing and possibly adhesion or transfer of asperities. Although both of these mechanisms were possible, it is not clear which of the two mechanisms was more influential in producing initial small debris. The generation of these initial wear debris was also confirmed by manually stopping the RCF test after a short period of time (few minutes) and analysing the test lubricants. Test lubricants indicated the presence of tiny wear debris of the coating material. These debris were generated long before the rolling element failed. Once these small wear debris were produced, the wear mechanism accelerated due to additional mechanism of three body abrasion which eventually lead to the failure of coated rolling elements. This mechanism of asperity contact and three body abrasion was further accelerated during the dry test (GG5AX) due to the absence of lubricant film within the contact region. However, the wear track at the end of RCF test was similar to the observations shown in Figs. 3 and 4. This indicated that the lubricant film effected the duration of the RCF test but did not significantly alter the mechanism of surface wear.

7.2.1. Evidence of adhesion

Surface observations of lower planetary balls (Fig. 7a) showed that WC debris were adhered (transferred) to the surface of steel planetary balls. Similar trend was observed with other tests conducted with steel lower balls. The size of these adhered debris was generally in the range of 1 μm. This indicated that asperity adhesion took place during the RCF tests. These debris were strongly adhered to the surface and did not come off during the ultrasonic cleaning (acetone bath) of lower planetary balls. This trend was however not so definite in the case of planetary ceramic balls. Except in one case, no debris were observed on the surface of lower ceramic balls. This difference was attributed to the differences in the metallurgy and surface chemistry of steel and ceramic balls.

7.2.2. Evidence of abrasion

Ploughing and three body abrasion on the lower planetary steel balls can be seen from Fig. 7(b). Abrasion on the wear track of planetary steel balls was attributed to the lower hardness (HV 850) of steel planetary balls in comparison to the hardness of coating (HV 1158). The WC debris produced during the test were approximated to be of the same or higher hardness than the hardness of the coating to further accelerate the process of abrasion. The process was however different in the case of lower ceramic planetary balls. Abrasion of planetary balls was negligible in the case of ceramic lower balls, which was attributed to the higher hardness of ceramic balls (HV 1580). This indicated that ceramic planetary balls outclassed the coatings due to their higher hardness resulting in lower RCF life of tests conducted in hybrid ceramic bearing configuration. Similarly, on the surface of wear track of failed coated rolling elements abrasion was observed as shown in Fig. 3(b)Fig. 4(b).

Fig. 12 shows a schematic of surface wear type of coating failure. The figure shows the initiation of wear debris at the asperity contact due to the above discussed mechanism and further acceleration of process due to action of wear debris. The behaviour of wear debris entering the contact area of rolling sliding contact is, however, complex depending upon the size, shape, composition, hardness, of debris and the tribological conditions within the contact region. No attempts were made to investigate the effect of shape and size of wear debris on the rate of surface wear process. Sayles (1995) [15] has given some description of influence of these factors.

It can be appreciated that when the RCF tests were conducted with Hitec-174 ($\lambda > 3$) as the test lubricant, the lubricant film should have fully developed completely separating the two surfaces thereby avoiding any asperity

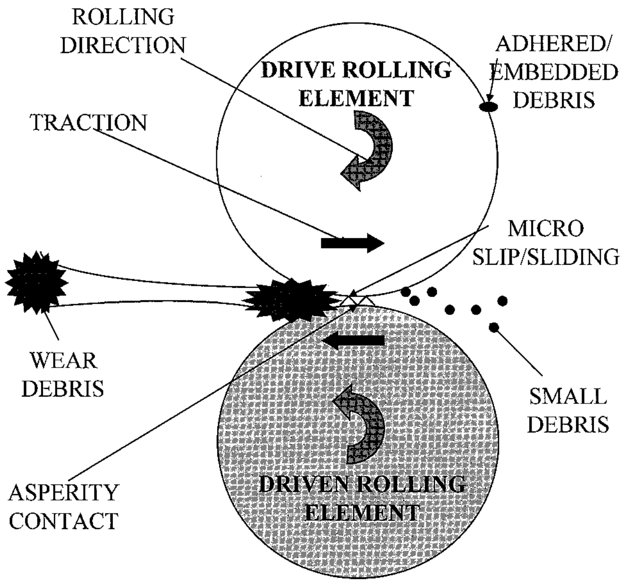

Fig. 12. Schematic of coating surface wear process.

contact. Thus surface wear should not be observed with this lubricant. However, surface observations indicated surface wear for the tests conducted with Hitec-174 lubricant. This difference between the lubrication regime and surface wear was attributed to the following reasons: (a) At the start of RCF tests the EHL film is not fully developed providing a possibility of asperity contact within the contact region. Also, the effect of running in period cannot be overlooked. (b) During the RCF tests theoretical film calculations indicate a value of λ in the range of 3 to 4. This marks the beginning of fully developed lubrication film. Slight changes in surface roughness and lubricant viscosity (due to flash temperature, friction) can cause this regime to migrate into the mixed region. These calculations were based upon the average root mean square (R_q) values of surface roughness. Some asperity peaks will always be higher then the average asperity height, which can provide an initial asperity contact leading to the generation of wear debris. Moreover, two-dimensional surface roughness parameters were used in the calculations of λ value.

In general, the mechanism of surface wear initiated from the generation of small debris due to asperity contact which accelerated the process of surface wear due to three body abrasion.

7.3. Coating delamination

Delamination was another type of failure seen on the surface of coated rolling elements. This type of failure was seen for the RCF tests conducted with both the lubricants. This is consistent with the previous studies by the authors [3]. When coated rolling element failed in delamination type failure the RCF performance was reduced (Table 1). Figs. 2 and 5 show typical surface observations of this type of failure. In this type of failure, larger chunks of coating delaminated parallel to the surface of the wear track resulting in sheet like debris as shown in Fig. 7(b). In the case of thinner coatings (coating thickness < 100 μm) this type of failure generally took place at the coating substrate interface (Fig. 5) at an approximate depth of maximum shear stress. The coating was defined thin if the coating thickness was such that the maximum shear stress was located at or below the coating substrate interface. However, in thicker coatings (coating thickness > 150 μm) the delamination took place from within the coating microstructure (Fig. 2). The coating was defined thick if the coating thickness was such that the maximum shear stress was located within the coating microstructure so that shear stresses did not influence the interfacial stresses. Surface observations indicated that the depth of delamination failures can either be approximated as 45 μm or 90 μm under the given test conditions. These depths can be related to the depths of orthogonal shear stress or maximum shear stress, respectively (Table 1).

7.4. Mechanism of coating delamination during the RCF test

Consider the subsurface observations of the failed coated rolling element cone GG3AX. In this case, the approximate coating thickness was 260 μm which can be classified as thick coating under the given test conditions. Fig. 10 indicates that subsurface cracks were initiated at the depth of maximum shear stress and orthogonal shear stress. The origin of these cracks was attributed to the stress concentrations owing to the micropores, microcracks, secondary phase particles as were seen in the coating microstructure (Fig. 8) which eventually resulted in the macro-pitting of surface. This was consistent with the work described by Littmann and Winder (1966) [16], in which subsurface inclusions and oxides were thought to be the cause of subsurface fatigue due to crack initiation and propagation at the depths of maximum shear stress and orthogonal shear stress. The stress concentrations due to the defects in the coating microstructure were also influential in poor behaviour of these coating during the microhardness/fracture toughness studies (Fig. 11). These studies revealed that coating cracked readily at low indentation loads (100 p) at some locations whereas resisted cracking at even higher loads at other locations. This difference is attributed not only to the variations in density of microstructural defects but also their shape and size. It was appreciated that the indentation load caused stress concentrations at the location of coating microstructural defects. This led to the cracking of the coating microstructure at low indentation loads. This also showed the difficulties in attaining the experimental data on the mechanical properties of these highly anisotropic thermal spray coatings.

During RCF tests of plasma sprayed rolling elements these cracks propagated at specific depths of shear stresses. These depths did not relate to the depth of layer per pass of spraying which, was approximated as 15–20 μm. This indicated that the coatings had poor shear strength and the crack propagation was in shear mode (mode II). However, the possibility of cracking in mode I or a combination of modes I and II cannot be excluded. The investigation of mode of crack initiation for a brittle, lamella and anisotropic coating microstructure was beyond the scope of this experimental work. The coating microstructure generally behaved in a complex way and it was even difficult to quantify the exact values of stress intensity factor, shear strength, etc. There is a significant scatter in published literature [17] on the mechanical properties of thermal spray coatings tested using different techniques. However, it was confirmed on the basis of these surface and subsurface observations and, the shape and size of debris that whatever was the mode of initiation/propagation, ''*the cracks propagated at the depth of maximum shear stress and orthogonal shear stress due to the stress concentrations owing to the defects in the coating microstructure under the applied contact load*''.

7.4.1. Crack propagation in thick coatings

Once these cracks were initiated they propagated at the specific depths of shear stresses. It was observed that the behaviour of crack propagation at two different depths of shear stresses was different. The cracks at the depth of maximum shear stress continued to develop in both directions either by the propagation of single crack or by the combination of small cracks at the same depth (Fig. 9b). When the location of these cracks became such that they occurred in the vicinity of another crack (at orthogonal shear stress), the cracks (at maximum shear stress) approached the crack at the depth of orthogonal shear stress. This was accompanied by a change in the direction of crack propagation towards the surface (Fig. 9c). In general, the cracks at the depth of maximum shear stress did not directly reach the surface. After the combination of the two cracks which initiated at two different depths, the combined crack generally propagated at the depth of orthogonal shear stress.

The independent cracks at the depth of orthogonal shear stress (Fig. 9e and g) propagated in the same manner as the cracks at maximum shear stress, i.e., parallel to the surface. However, these cracks were generally shorter in length and eventually reached the surface after reaching a certain crack length. This resulted in delaminating the coating at the depth of orthogonal shear stress (approximately 45 μm) for thick coatings (Fig. 9f).

7.4.2. Crack propagation in thin coatings

The mechanism of crack propagation in thin coatings was different to thick coatings. Consider the subsurface observations of the rolling element cone GG2BY (Fig. 10). In this case, the coating thickness was approximately 80 μm. The coating can thus be regarded as thin coating, i.e., maximum shear stress was located near the coating substrate interface. The initiation and propagation of these cracks was attributed to the same factors as described above with the additional effects of stress concentrations caused by the mismatch of coating and substrate properties at the interface. This effect of mismatch of the mechanical properties (Young's modulus, Poisons ratio) and the possibility of the presence of inclusions, contamination layers at the interface provided an acceleration in the crack initiation and propagation at the interface. Therefore, in the case of thinner coatings the cracks at the depth of maximum shear stress (located at the interface) initiated and propagated much quicker than the cracks at the orthogonal shear stress. These cracks reach the surface either independently leading to coating delamination at the interface or after joining with cracks at orthogonal shear stress. Fig. 10(c) shows a view in which both types of delamination are visible. However, in most of the cases of thinner coatings interfacial cracking and interfacial delamination were common. The poor performance of thinner coatings can thus be understood by the accelerated crack propagation at the coating substrate interface.

The mechanism of delamination for thick and thin coatings can thus be summarised as follows.

(1) Cracks were initiated at different depths under the wear track and propagated at the depths of maximum shear stress (90 μm) and orthogonal shear stress (45 μm). For thicker coatings, these cracks were located within the coating microstructure and for thinner coatings within the coating microstructure as well as at the coating substrate interface.

(2) These cracks were initiated at stress concentrations due to micropores microcracks and secondary phase particles within the coating microstructure. An additional factor of mismatch of properties at the interface and possibility of contaminant layer was also influential which accelerated the crack propagation in thin coatings.

(3) For thicker coatings (coating thickness > 150 μm), these cracks propagated slowly at their respective depths within the coating microstructure. However, for thinner coatings (coating thickness < 100 μm) the cracks at the coating substrate interface propagate much faster than the cracks at orthogonal shear stress.

(4) For thicker coatings, the cracks at maximum shear stress extend to greater lengths until they meet a crack at the depth of orthogonal shear stress by changing its direction. For thinner coatings, the cracks at interface had the greater tendency of reaching the surface independently. However, in some cases, they combined with the cracks at the depth of orthogonal shear stress and eventually reached the surface.

(5) For thicker coatings the cracks from the depth of orthogonal shear stress reach the surface much quickly than the cracks at the depth of orthogonal shear stress

thereby leading to coating delamination at the depth of orthogonal shear stress. In the case of thinner coatings, the effect was generally the opposite and interfacial delamination took place at the location of maximum shear stress.

A schematic of this delamination process is shown in Fig. 13 for both thick and thin coatings. The figure summarises schematically the mechanism of delamination during the RCF tests based on the location and orientation of subsurface cracks. These observations indicate that the coating delamination was a subsurface failure mechanism resulting in macro-pitting of surface due to subsurface cracks which nucleated from coating defects. The subsurface investigations of the coated rolling elements which did not fail in delamination revealed no subsurface cracks. This showed that the coatings which did not delaminate actually resisted the subsurface cracking.

It is the authors' view that during the RCF test there was a competition between the two modes (surface wear and delamination) of failures. In the early stages of RCF tests, the contact stress was high and there was a high tendency towards delamination type failure. This can be appreciated from the test results (Table 1) in which delamination type failures were generally associated with lower RCF life. If the test conditions were such that the coating microstructure resisted this delamination failure in the early stages of RCF test, surface wear decreased the tendency towards delamination type of failure in the later stages of RCF test. This was due to the decrease in contact stresses as a result of contact conformity brought about by the surface wear.

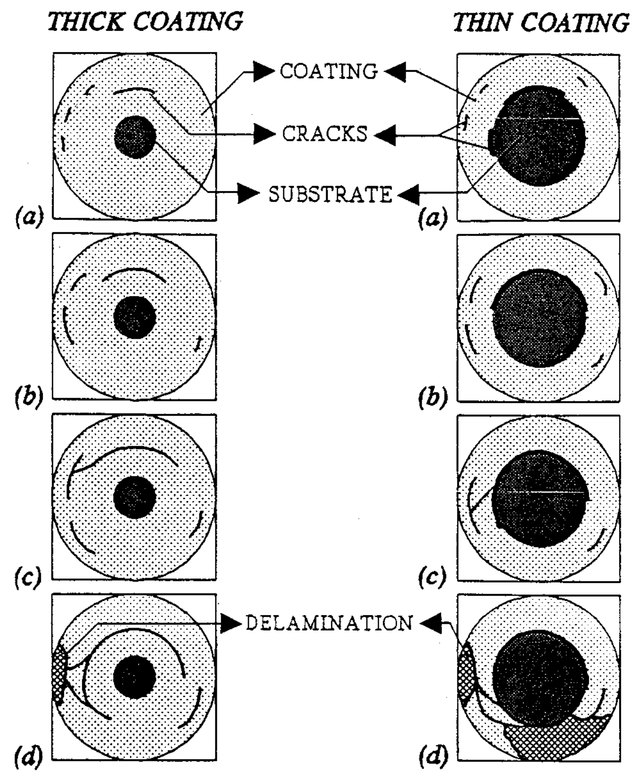

Fig. 13. Schematic of coating delamination process. (a, Initiation of cracks at the depths of maximum shear and orthogonal shear stress; b, propagation of cracks parallel to surface; c, combination of cracks; d, coating delamination.)

7.5. Possibilities of lubricant entrapment mechanisms

Surface initiated fatigue crack propagation due to lubricant entrapment has been an area of debate ever since the pressurising mechanism was suggested by Way [18]. Way suggested that the oil penetration of very small surface cracks with a certain initial direction was the reason for the growth of fatigue cracks until the particle was separated from the body of the rolling element. Although the subsurface observations strongly suggested that coating delamination was a subsurface mechanism, it was important to explore the possibilities if lubricant entrapment could have significantly contributed to the coating delamination. The complexity of the problem is mainly due to the effects of surface roughness and topography, lubricant viscosity, residual stresses, magnitude and direction of traction and asperity behaviour, which should be considered concurrently with this mechanism. Many researchers have experimentally and analytically tried to study the effects of some of the above factors but the complexity caused by the above mentioned tribological factors have made it difficult to confidently conclude this theory. Yet the experimental evidence suggests that cracks only propagate in the presence of lubricant and if traction is present in the preferred direction of load movement [19]. After Way's theory, later researchers suggested additional mechanisms to support this theory by considering a mode II crack propagation due to reduced coefficient of friction at the crack tip in the presence of lubricant causing the surfaces to slide. Others suggested the mechanism of lubricant entrapment leading to hydrostatic pressure build-up causing the crack tip to open in mode I and then in mode II due to the leakage of the entrapped lubricant. In general, there is substantial awareness of the possibility of lubricant related crack propagation. The actual mechanism(s) of lubricant initiated crack propagation leading to fatigue failure is, however, beyond the scope of this work. The above mentioned mechanism of coating delamination concluded that the mechanism of crack initiation and propagation was subsurface due to stress concentrations. It can, however, be established on the basis of current and previous investigations that even if lubricant entrapment was operational during the RCF tests, it is not likely to be an influential mechanism leading to coating delamination on the basis of the following observations.

(a) The delaminated coating and subsurface cracks extended much beyond the width of the wear track as seen in Fig. 9(a). This cannot be explained by the mechanism of hydrostatic pressure build-up as the stresses will be tensile at the edge of the wear track.

(b) Cracks occurred subsurface and only at specific depths and travelled circumferentially parallel to the surface.

(c) Delamination occurred with both lubricants and considering the extremely high viscosity of Hitec-174 (200 cSt), it does not seem likely for this lubricant to penetrate the cracks. This is consistent with the previous studies by the authors in which delamination occurred with Hitec-174 lubricant during the first few seconds of RCF test.

(d) The cracks were observed to propagate and reached the surface opposite to the direction of rolling in which case lubricant should be squeezed out of any surface originated crack thereby reducing the tendency of any fluid entrapment.

(e) The cracks were long (up to 7 mm in length) and it will require a very high load and extremely low viscosity oil to cause pressure build-up at the tip of these cracks.

(f) Tests conducted with dye penetrant (GG6AX) as the test lubricant did not delaminate. This test was specifically geared to investigate hydraulic fluid entrapment studies.

(g) Previous studies have shown that cracks can only surface beyond the edge of the wear track [3], which cannot be explained on the basis of the lubricant entrapment mechanism.

(h) The delaminated debris were of constant thickness with straight edges whereas if the crack was from surface to subsurface it should be inclined at approximately 30° to 45°.

The mechanism(s) of lubricant initiated crack propagation may or may not be present but the above observations indicate that the likelihood of such mechanism(s) significantly effecting the coating delamination was very rare. This is consistent with the results published by Nieminen et al. [20], when they reported that subsurface cracking of the coated rolling elements during the dry tests. Those studies revealed that there was no possibility of lubricant entrapment mechanism to aid the delamination crack propagation in thermally sprayed rolling elements.

8. Conclusions

The failure modes of WC–15%Co coated rolling elements thermally sprayed by high velocity plasma spraying were experimentally investigated using a modified four ball machine. Failure modes were classified on the basis of surface and subsurface investigations. The following conclusions were made.

(1) Two modes of failures, i.e., *surface wear* and *coating delamination* were observed on the surface of failed coated rolling elements. These rolling elements failed in either one or a combination of these two modes.

(2) Surface wear was associated with asperity contact in the presence of microslip/sliding within the contact region and resulted in micro-pitting of surface. The process was accelerated in the later stages of RCF tests in the presence of wear debris due to additional mechanism of three body abrasion.

(3) Coating delamination was associated with the initiation/propagation of subsurface cracks, which originated from various defects either within the coating microstructure or at the coating substrate interface and resulted in macro-pitting of surface. These cracks propagated at the depths of orthogonal shear stress and maximum shear stress under the surface of wear track.

(4) Thinner coatings delaminated faster due to interfacial cracking as a result of mismatch of coating and substrate properties and due to the location of maximum shear stress at the coating substrate interface.

(5) Coating delamination generally occurred in the early stages of RCF tests, i.e., when the contact stresses were high. The tendency of this mode of failure was minimised in the later stages of RCF tests due to a decrease in contact stresses as a result of contact conformity due to surface wear.

(6) It was observed that the probability of lubricant entrapped mechanism of crack propagation leading to coating delamination was very low.

References

[1] Pawlowski, The Science and Engineering of Thermal Spray Coatings, ISBN 0-471-95253-2, 1995.
[2] R. Ahmed, M. Hadfield, Rolling contact fatigue behaviour of thermally sprayed rolling elements, Surface and Coatings Technology 82 (1996) 176–186.
[3] R. Ahmed, M. Hadfield, Rolling contact fatigue performance of detonation gun coated elements, Tribology International 30 (2) (1997) 129–137.
[4] R. Ahmed, M. Hadfield, Wear of HVOF coated cones in rolling contact, Wear 203–204 (1997) 98–106.
[5] S. Tobe, S. Kodama, H. Misawa, Rolling Fatigue Behaviour of Plasma Sprayed Coatings on Aluminium Alloy, Tokyo Metropolitan University, 2-1-2, Fukazwa, Setagaya-Ku, Tokyo, Japan, 1990, p. 158.
[6] P. Sahoo, High performance wear coatings—the quest continues, Powder Metallurgy International 25 (1993) 73–78.
[7] A. Makela, P. Vuoristo, M. Lahdensuo, K. Niemi, T. Mantyla, Rolling Contact Fatigue Testing of Thermally Sprayed Coatings, Conference Proceedings, Thermal Spray Industrial Applications, 1994, pp. 759–764.
[8] M. Yoshida, K. Tani, A. Nakahira, A. Nakajima, T. Mawatari, Conference Proceedings, International Thermal Spray Conference, Kobe, Japan, 1995, pp. 663–668.
[9] B.O. Jacobson, Rheology and Elasto-hydrodynamic Lubrication, Baker and Taylor, 1991.
[10] R. Ahmed, M. Hadfield, Rolling contact fatigue performance of plasma sprayed coatings, Wear, (1998) in print.
[11] Engineering Science Data Units, ESDU 84017, 1984.
[12] M.D.F. Harvey, A.J. Sturgeon, F.J. Blunt, S.B. Dunkerton, Investigation into the relationship between fuel gas selection, wear performance, and microstructure of HVOF sprayed WC-Co coatings, International Thermal Spray Conference, Japan, 1995, pp. 471–476.
[13] V.H.S. Wilms, The microstructure of plasma sprayed coatings, Ph.D. thesis, SUNY at Stony Brook, 1978.
[14] V.V. Kudinov, P. Pekshev, V.A. Safiullin, Forming of the structure of plasma-sprayed materials, High temperature dust laden jets, 1989, pp. 381–418.

[15] R.S. Sayles, Debris and roughness in machine element contacts: some current and future engineering implications, Journal of Engineering Tribology 209 (3) (1995) 149–172.
[16] W.E. Littmann, R.L. Winder, Propagation of contact fatigue from surface and subsurface origins, ASME Transactions 624–636 (1966) .
[17] O.C. Brandt, Mechanical properties of HVOF coatings, Journal of Thermal Spraying 4 (1995) 147–152.
[18] E. Way, Pitting due to rolling contact, Journal of Applied Mechanics 2 (1935) A49–A58.
[19] A.F. Bower, The influence of crack face friction and trapped fluid on surface initiated rolling contact fatigue cracks, ASME Transactions 110 (1988) 704–711.
[20] R. Nieminen, K. Vuoristo, K. Niemi, T. Mantyla, Rolling contact fatigue characteristics of thermal spray coatings, National Thermal Spray Conference, Houston, USA, 1995, pp. 651–657.